NON-LINEAR DYNAMICS SIMULATION-BASED TESTING TO CREATE OPERATING ENVELOPES FOR AUTONOMOS UAS INSPECTION MISSIONS

Vincent Page, v.page@liverpool.ac.uk, University of Liverpool, United Kingdom

Christopher Dadswell, c.m.dadswell@liverpool.ac.uk, University of Liverpool, United Kingdom

Mike Jump, mjump1@liverpool.ac.uk, University of Liverpool, United Kingdom

Abstract

This paper uses stitched linear and non-linear models to simulate the dynamics of an autonomous TRex-700E model helicopter in order to determine its operating envelope. The helicopter is simulated carrying out an oil rig inspection mission and the wind speed and direction are used to define its operating limits. These limits were determined by applying a series of cost functions, which use operator set performance requirements, to the velocities, attitudes, controls inputs, and position of the UAS over the course of the mission. It was found that for benign wind conditions, in this case <10 knots wind speed, the linear models provide a reasonable approximation. However, as the operating limits reached, the non-linear and linear models diverge. Therefore, to determine the operating limits in harsher wind conditions, the non-linear models would be required.

1. INTRODUCTION

There is currently a drive to use autonomous systems to aid in offshore operations [1]. The ORCA Hub is a multimillion-pound programme aimed at addressing the offshore energy industry's vision for a completely autonomous offshore energy field. This vision arises from the need to reduce costs and risk associated with offshore energy asset operations and maintenance. One area of interest is the use of aerial robots to perform inspection of the offshore energy assets.

The offshore environment can be characterised by dynamic winds, high sea states, turbulent air wakes from offshore assets, and distant operations, see *Figure 1*; therefore, any autonomous aircraft would be required to operate by itself in this potentially hostile environment. A common concern for this concept of operations is that the autonomous system will not be safe to use in such a situation.

Safety assessments for manned rotorcraft operations in the offshore environment have typically assessed the operating limits of the aircraft via piloted trials [2]. However, this is expensive and can potentially be dangerous. The University of Liverpool has a significant track record in the development and use of flight simulation to de-risk the process of generating Ship-Helicopter Operating Limit (SHOL) diagrams [3]–[7]. SHOL diagrams, also known as operating envelopes, define the wind conditions that a particular aircraft can safely perform operations to or from a particular ship. An example of such a SHOL diagram is given in Figure 2. This process requires the use of a subjective pilot assessment metric to rate the environmental conditions and their impact on task completion, such as the DIPES scale [3]. However, since these techniques require the presence of a pilot to determine operational safety at a particular condition, they are therefore currently unsuitable for use with autonomous systems. As part of the Verification and Validation (V&V) (and ultimately certification) process required of any autonomous system, a similar safety assessment process is needed for the envisaged offshore inspection missions.

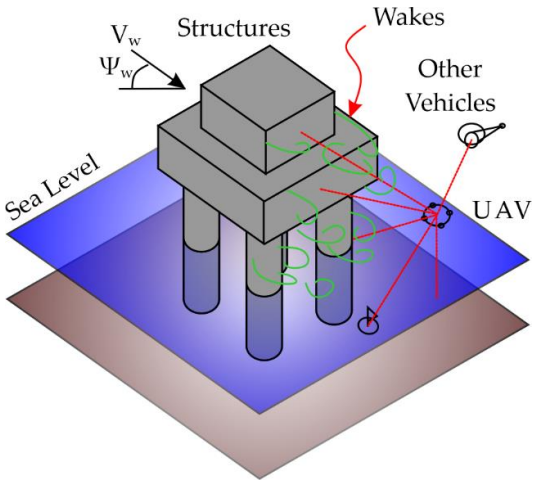

Figure 1: UAS operating environment for the selected mission scenario

By using the manned SHOL-generation process as its inspiration, previous papers by the authors [8], [9] presented a method that uses a series of cost functions to analyse the response of an autonomous rotorcraft in comparison to user defined specifications while it carries out a mission to perform an aerial inspections of a generic oil rig. A cost function was applied to each subsystem within the Guidance Navigation and Control (GNC) system of

Presented at 47th European Rotorcraft Forum, United Kingdom, 7-9th September, 2021

the aircraft (controller, guidance and actuators), thus differentiating the performance of each. Many faster-then-real-time simulations of the same mission were carried out under a wide range of wind conditions and the cost functions were used to determine the performance limits of the system. This approach was tested using stitched, linearised state-space models in steady wind conditions intended to emulate the full domain of a nonlinear model.

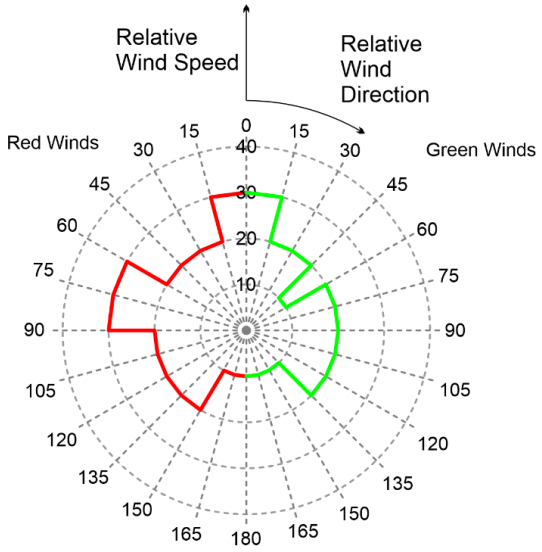

Figure 2: A generic example SHOL that would be generated for a helicopter ship landing manoeuvre

The stitched linear models execute more quickly than a full nonlinear model, but their lower modelling fidelity may have significant impact on the overall operating limit predictions made. It is unclear whether this deficit in modelling fidelity will significantly affect the outcome of the operating envelope generation procedure, and hence whether more computationally expensive non-linear modelling techniques are required for all or part of the process. If the linear models are adequate, then this allows for a greater number of conditions and mission types to be tested within a given timescale. This, in turn, will enable the reduced reliance on complex and expensive nonlinear modelling tools.

This paper will report on a study to determine how different, or indeed similar, the predicted operating limits are for an Unmanned Aerial System (UAS) oil-rig inspection mission generated using nonlinear and stitched linear modelling techniques. It is hypothesised that for routine flight conditions, i.e. low wind speeds, the linear aircraft modelling will provide an adequate approximation of the aircraft response. It is argued that the lower model fidelity would be acceptable because, for practical reasons, the aircraft is unlikely to be operated at the edge of the envelope. However, to be able to predict the edges of the envelope, it is likely that the higher fidelity of the non-linear models will be required.

2. METHODS

In Ref. [9] a system that simulates the flying of a small unmanned helicopter was described. The helicopter was tasked with flying around the legs of an oil rig autonomously. The dynamics of the aircraft were calculated using stitched linear models. The models were stitched using the forward flight speed, wind magnitude and wind direction as inputs. This is an abstraction that was made to speed up the simulations in order to verify that the autonomy used to follow the path and fly between the legs of the oil rig does so within the performance specification defined by the user.

In this paper, a non-linear model was used instead of the stitched linear models. The same analysis process is applied to the simulation results as in the previous paper. The controller, guidance, and navigation system are the same between the linear and non-linear simulations, only the flight model differs.

2.1. Non-Linear Aircraft model

The airframe used for this investigation was chosen as the Align T-Rex 700E, a small aerobatic “3D” helicopter, often operated as a Remotely Piloted Aircraft (RPA) for sport flying. This particular vehicle was chosen as a representative aircraft of similar scale to that which may be used in offshore inspection tasks. The T-Rex 700E has a 2-bladed rotor with a diameter of 1.582m, has a maximum take-off mass of 5.2kg and can be retrofitted with a range of systems to enable autonomous operations.

The University of Liverpool maintains a simulation model of the T-Rex built in FLIGHTLAB, a state-of-the-art, physics-based, selective fidelity modelling and analysis software package [10]. The nonlinear FLIGHTLAB model was generated as a scaled version of a Yamaha R-MAX model, a similarly configured but larger aircraft, which has been partially validated against flight test data. The T-Rex model is comprised of a number of separate component models representing the different parts of the aircraft which are illustrated in Figure 4: a blade-element model of the main rotor with a Peters-He inflow model, a Bailey tail rotor model, aerodynamic lookup tables to generate forces from the fuselage, and a stability bar modelled as a rate feedback gain in the roll and pitch axes. The FLIGHTLAB software suite includes tools for trimming this model in given flight conditions, performing responses to defined control inputs, generating linear state-space models and running real-time simulation tests.

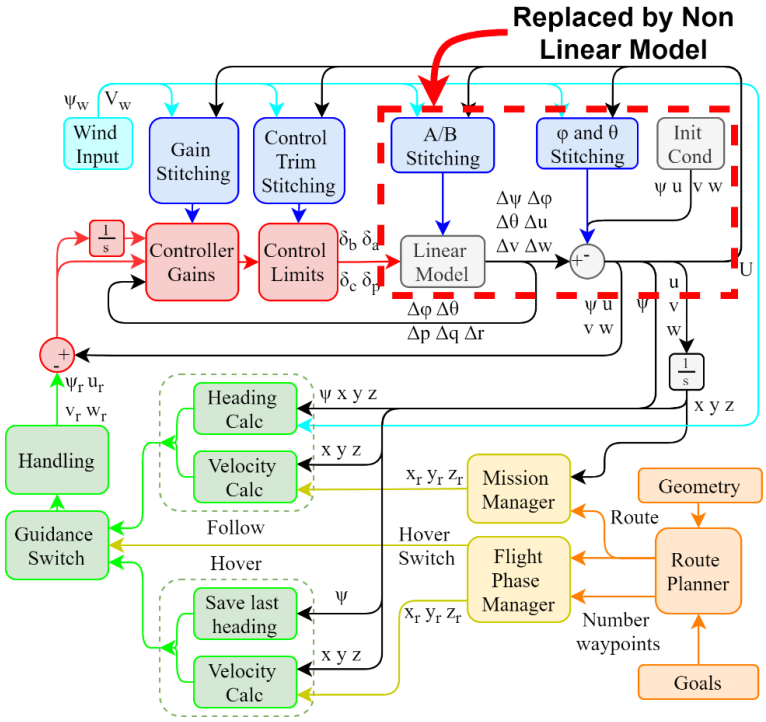

Figure 3: System diagram of the simulator used with the parts replaced by the non-linear model indicated

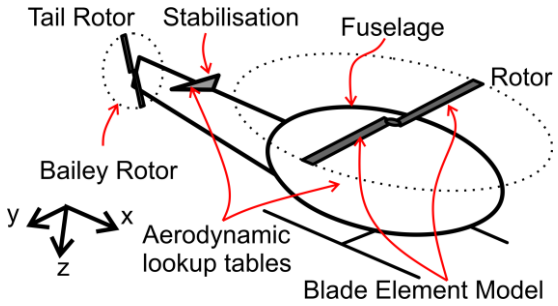

Figure 4: Overview of FLIGHTLAB nonlinear model components and the simulation models they use

The nonlinear FLIGHTLAB model has been interfaced with the control and guidance system developed in Matlab/Simulink via an SDX pipeline. SDX is a semaphore-based interprocess communications protocol for 'lock-step' synchronisation between FLIGHTLAB and other simulation programs [11]. This communication system ensures that the two separate models run at the same rate in real-time and that results are repeatable. The process uses a data block in memory of a pre-defined structure to 'put' or 'get' data from memory on each side of the SDX pipeline. This process was implemented in Matlab/Simulink through a custom S-function written in C. A matching set of FLIGHTLAB scripts was written to trim the aircraft in a required flight condition, initialise the data blocks to be exchanged with Simulink, add SDX calls to the model cycle function and then run the simulation model for a period of time in conjunction with the control and guidance system.

2.2. Stitching and linearization

The linear models were derived from the non-linear model using FLIGHTLAB's linearization tool. The attitudes, ground body velocities and attitude rates were taken as the states of the linear models. They were then stitched together by using interpolation between each element of the A and B matrices for each of the operating points, see Figure 5. The operating the points the models were linearized at are given in Table 1. The linear model matrices are then updated as the simulation progress and the flight conditions transition between operating points.

Table 1 Operating points used for the model linearisation

Operating Condition	Range of Values (Min:Delta:Max)
Forward Velocity U	−20:5:40
Wind Speed V_w	0:5:40
Wind Direction ψ_w,	0:30:330

The process of linearisation simplifies dynamics of the helicopter and is only valid at the operating point it was linearised at. The stitching process aims to mitigate this simplification by using the models at nearby operating points to predict the dynamics at in between flight conditions. This is,

however, an imperfect process and some detail in the dynamics is still lost. It is currently unclear though whether this actually results in an operating envelope that is significantly different from the non-linear models.

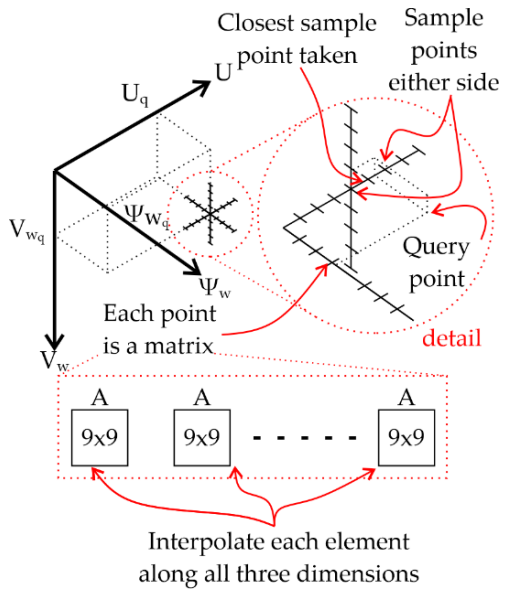

Figure 5: Linear model stitching methodology

2.3. Mission Success Metrics

To assess manned flight missions the DIPES scale is often used [3]. However, the equivalent for the autonomous operations does not exist. In Refs. [8] and [9] a set of cost functions were developed to fill this gap. These cost functions are applied to each segment of a mission, where a segment is the time between waypoints. The worst performing segment is used to characterise the performance of the autonomous system.

The actuator, controller, and guidance subsystems have their own cost functions. These cost functions are aimed at evaluating the subsystem based on what it is tasked with doing. As such the actuator is tasked with providing control authority, the controller with maintaining stability and tracking the desired stated and the guidance with following the desired path.

The cost functions use user specifications to calculate the performance. This is so that the user, which may be the engineer designing the system or a regulator determining the safe operation of it, can set the level of performance the helicopter needs to meet. The functions used here were developed in Refs. [8] and [9] and are repeated here briefly.

Figure 6 and equation (1) show how the actuator performance is determined, where it is required to have excess control authority in order to cope with sudden requirements.

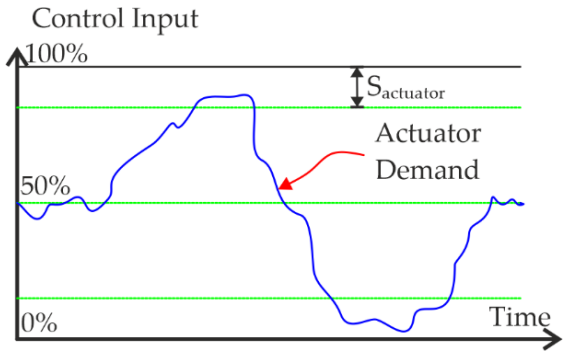

Figure 6. Definition of the cost function for the analysis of the actuator's performance

$$(1)\quad F(\bar{\theta}) = F_A = \max\left(\frac{1}{t_m}\int_0^{t_m}\frac{\sqrt{\left(\bar{x}_{actuator_i} - 0.5\right)^2}}{0.5 - \bar{S}_{actuator_i}}dt\right)$$

where t_m is the segment simulation time, $x_{actuator_i}$ is the *i*th actuator output at time t, $\bar{S}_{actuator}$ the specified margin of error, and dt is the time step of the simulation.

Figure 7 and equation (2) give the cost function for the controller and is based on the cost function for LQR controller tuning methods [12]. The controller is assessed on its ability to follow the tracking variables, in this case the ground body velocities and helicopter heading.

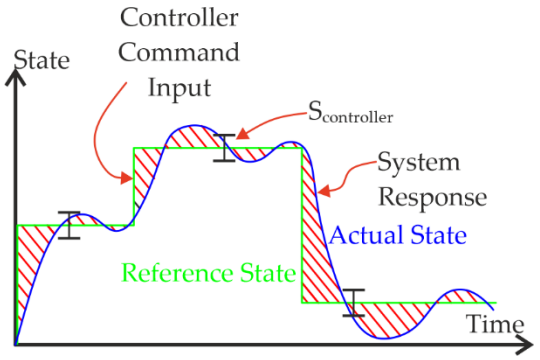

Figure 7: Definition of the cost function for the analysis of the controller's performance

$$(2)\quad F(\bar{\theta}) = F_C = \max\left(\frac{1}{t_m}\int_0^{t_m}\frac{\sqrt{\left(\bar{x}_{reference_i} - \bar{x}_i\right)^2}}{\bar{S}_{controller_i}}dt\right)$$

Where $\bar{x}_{reference_i}$ is the command reference, $\bar{x}_i$ the measured state of the system, and $\bar{S}_{controller_i}$ the specified maximum difference between the actual and reference values.

Finally, Figure 8 and equation (3) shows the performance measure for the guidance subsystem, which is assessed on its ability to follow the path within a set deviation.

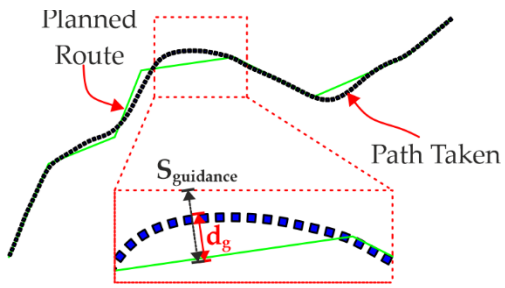

Figure 8: Definition of the cost function for the analysis of the guidance performance

(3) $$F(\bar{\theta}) = F_G = \frac{1}{t_m}\int_0^{t_m} \frac{d_g}{\bar{S}_{guidance}} dt$$

where d_g is the perpendicular distance from the actual position to the desired path and $\bar{S}_{guidance}$ is the specified maximum deviation from the path.

These performance measures are applied to the autonomous system using either the non-linear or linear models to calculate the dynamics. The specifications used are shown in Table 2.

Table 2: Performance Specifications used with the cost functions

$\bar{S}_{Actuator} = 20\%$
$\bar{S}(1)_{Controller} = 5.5^o$
$\bar{S}(2:4)_{Controller} = 0.3\ m/s$
$\bar{S}_{Guidance} = 0.875\ m$

Each simulation output is split into segments the cost functions above are then applied to each of those segments. The segment that has the highest maximum cost is then taken as the performance of that subsystem for the entire mission. When the cost is higher than 1, then the subsystem has been deemed to have failed to meet specification.

2.4. Test Matrix

The test matrix used to compare the non-linear and linear models is shown in Table 3. This matrix is in essence all the permutation of the variations in wind speed and magnitude between 0 and 40 knots and 0 and 360°. The mission to be flown by the UAS is shown in Figure 9. From this matrix and the cost functions described in the previous section, the wind conditions at which the UAS is able to fly while satisfying the requirements that the user has imposed upon it can then be determined.

Table 3: Conditions the linear and non-linear models were both tested at

Variable	**Wind Speed**	**Wind Direction**
Range	$5 \geq V_w \leq 40$	$0 \geq \psi_w \leq 355$
Step	$\Delta 1$	$\Delta 5$
Total Variations	40	72
Total Combinations	2880	

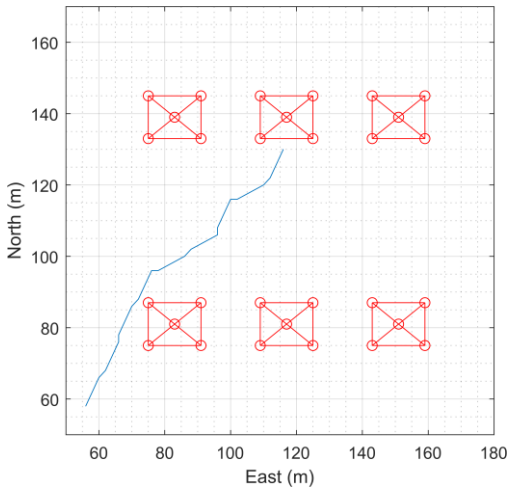

Figure 9: Route to be followed during the mission

2.5. Creation of Envelopes

For each test point in the matrix, values from each subsystem's cost function are assigned. The boundary of the envelope for each subsystem is then defined as the first wind speed at which the cost goes above 1 for a particular wind direction. This process is repeated for each wind direction within the test matrix until a continuous envelope is formed. The envelope must be contiguous; there can be no holes within the operating envelope.

2.6. Parallel Setup

To gather the simulation data in a reasonable timeframe the coupled FLIGHTLAB-Simulink system was parallelised to allow many simulations to be run at the same time and reduce overall processing time. To achieve this, a parallel pool of workers was created in MATLAB using the Parallel Computing Toolbox [13]. Each worker independently created a Simulink model, an instance of FLIGHTLAB and a corresponding SDX pipelines to allow communication between the two separate processes. The full test matrix was divided amongst the parallel workers so that each one computed a subset of the whole. This system was implemented on a desktop computer with an AMD Ryzen 9 3950X processor with 16 physical cores, and 32 usable processing threads. Only 16 processing threads were utilised in the parallel pool to prevent overloading of the CPU, since each simulation instances required a Simulink process and a FLIGHTLAB process to run. The parallel processing setup is illustrated in Figure 10.

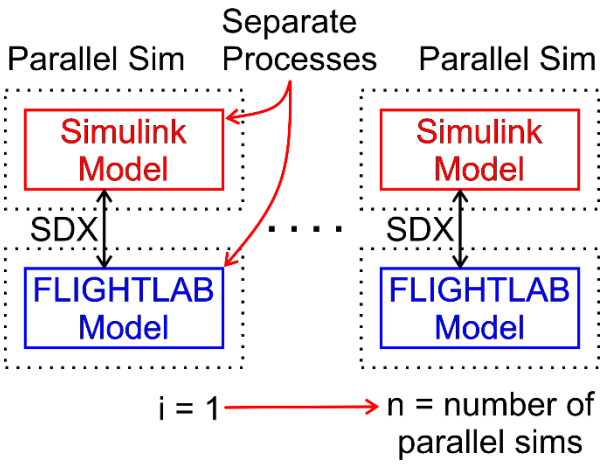

Figure 10: MATLAB parallel processing system used to simultaneously execute coupled FLIGHTLAB-Simulink simulations

3. RESULTS

Any differences between the stitched linear and non-linear flight models will be assessed by comparing the open loop and closed loop response of the aircraft. The closed loop responses use the autonomous system shown in Figure 3. Afterwards, the complete envelopes are compared to examine the differences after the verification phase and to determine whether the non-linear dynamics are required to complete a full envelope.

3.1. Open loop comparison

A comparison between the linear and non-linear open loop response is given in Figure 11 and Figure 12. Figure 11 shows the response of the aircraft to a 2% doublet input starting at 1 sec and ending at 3 seconds in lateral cyclic. Figure 12 gives the response to an identical input to the longitudinal cyclic. The linear response is shown in red while the non-linear response is blue.

The agreement between the models is favourable, where differences in the later parts of the response are mostly due to the drift from the trim state. The longitudinal input response appears to have slightly better agreement. This is likely due to the linear models being stitching using the forward flight speed.

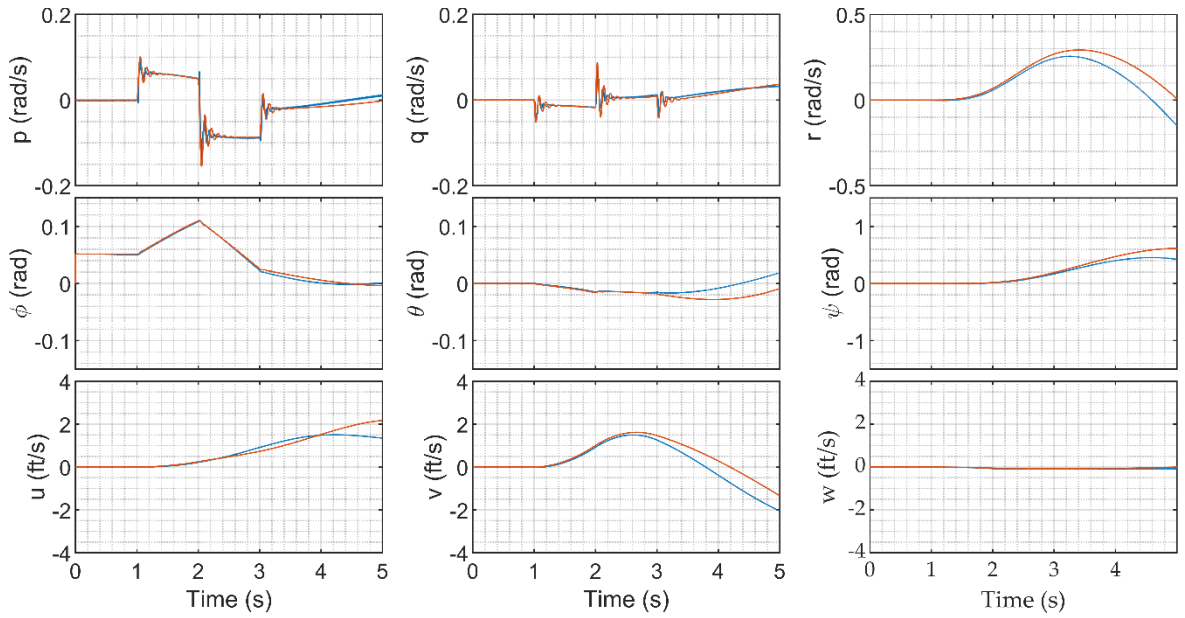

Figure 11: Nonlinear (blue) vs. linear (red) open loop response of the T-Rex700E to a 2% doublet input on the lateral control in hovering flight.

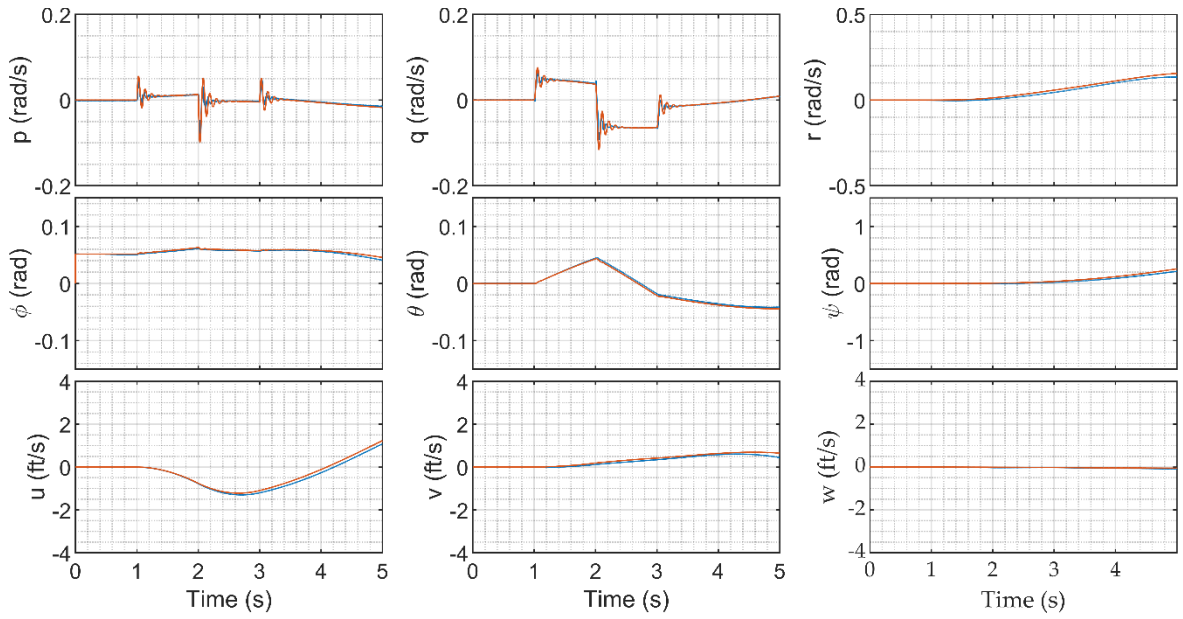

Figure 12: Nonlinear (blue) vs. linear (red) open loop response of the T-Rex700E to a 2% doublet input on the longitudinal control in hovering flight.

3.2. Closed loop comparison

The closed loop response is shown in Figure 13 through Figure 15. The flight conditions are a 1 knot wind from a heading of 135º with the aircraft following the route shown in Figure 9. As with the open loop response, the agreement between the models is favourable. As the mission progresses, there is an increase in the error between the models, but this is likely due to the accumulation of the differences over a mission that is taking around 2 minutes to complete. This manifests as a slight phase difference between the models in the latter stages of the mission.

There are slight magnitude differences in the phi and v states after the phase difference is accounted for. This matches with the comparison seen in the open loop response, where the lateral axis agreement is less than in the longitudinal axis. This magnitude difference also occurs in the comparison of the control authority.

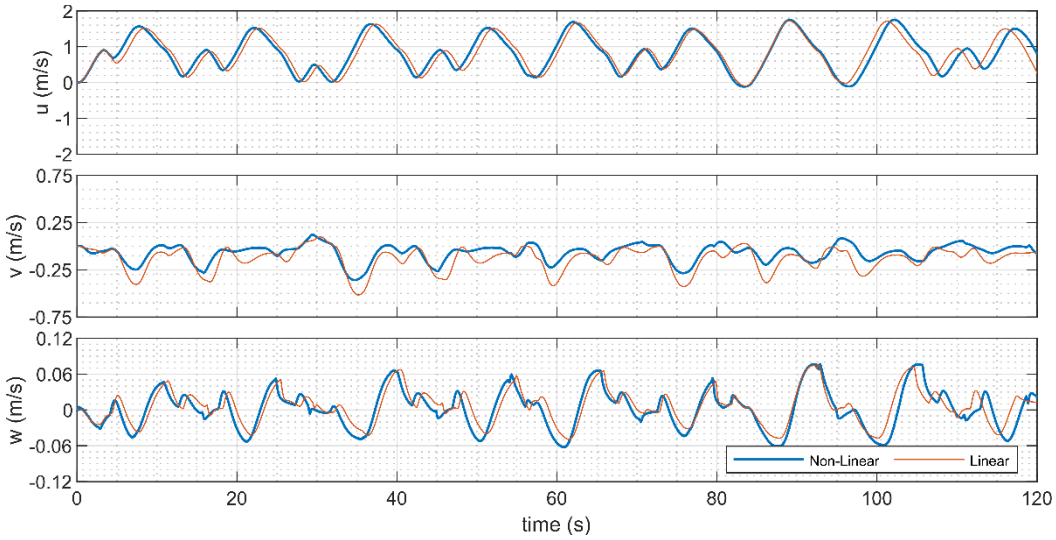

Figure 13: Closed loop response of ground velocities for linear and non-linear models $\psi_w = 135$ and $V_w = 1$.

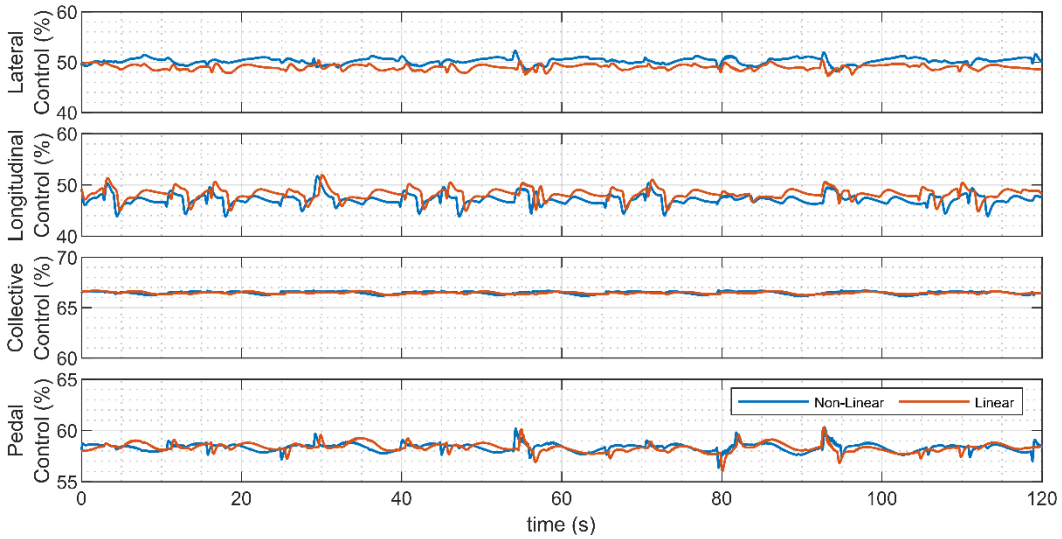

Figure 14: Closed loop response of controls for linear and non-linear models $\psi_w = 135$ and $V_w = 1$.

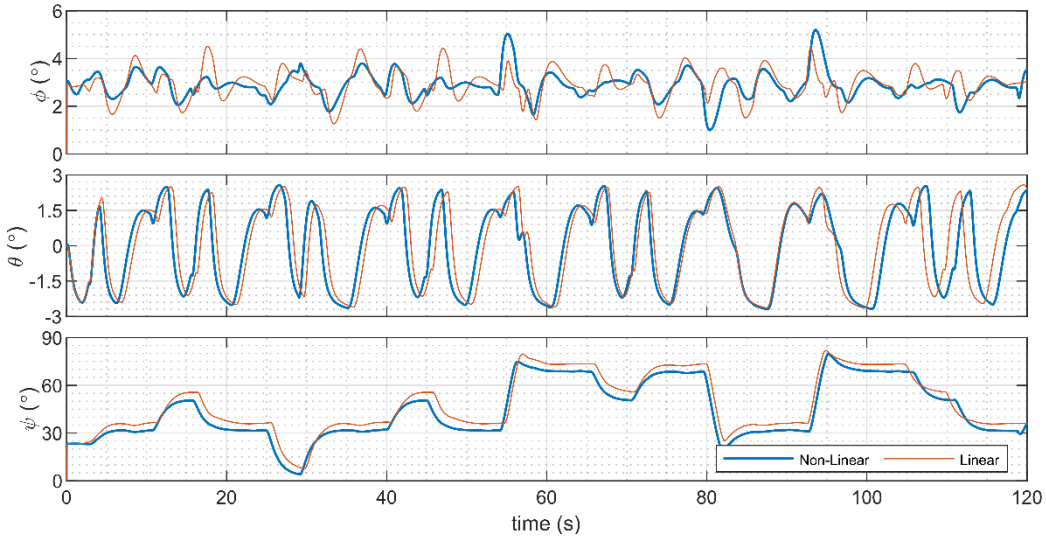

Figure 15: Closed loop response of attitudes for linear and non-linear models $\psi_w = 135$ and $V_w = 1$.

3.3. Envelope comparison

In this section the envelopes for the two models are compared. For each test point within the test matrix Figure 16 and Figure 17 show the simulation outcome for each model respectively, where blue denotes a complete and successful simulation, green where a mission was not completed, yellow where the mission resulted in an unstable aircraft, and red where the simulation started outside the trim envelope of the aircraft and was not attempted.

It can be seen clearly that there is a difference between the two models. The north and north east regions seem to be similar, while the south, and west differ, which correspond to when when the wind is coming either behind the helicopter or from the sides. For the non-linear model there are far more out of trim results. This is because the linear models estimate the trim states from the stitching process, as they are on a coarser grid than the test matrix. The non-linear models trim for every test point, thus will completely reject test points where trim is not possible. The linear models estimate the trim states and will attempt the mission regardless of whether the estimated trim state is viable or not, leading to a critical failure, rather than a trim failure.

Between Figure 18 and Figure 19 the subsystem envelopes are compared. It can be seen that the differences in simulation outcome are borne out here as well. In the north and east regions, the agreement for the guidance and actuator subsystem is favourable, if with slight differences, while for the controller however, there is considerable difference between the envelopes. In the south and east regions, there is little agreement for wind speeds greater than 10 knots.

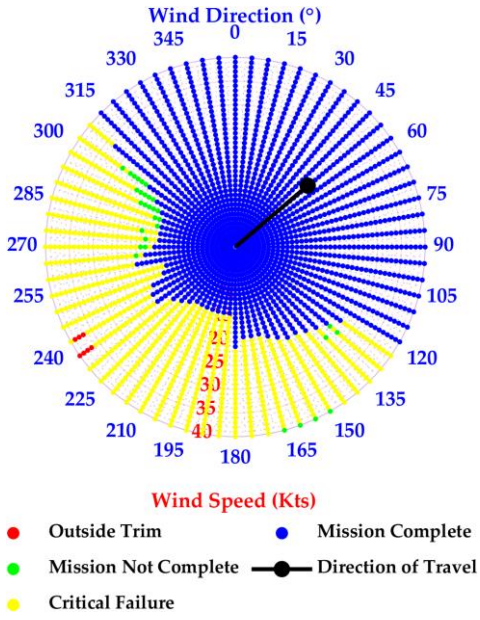

Figure 16: Simulation outcome tracking for the linear model simulations

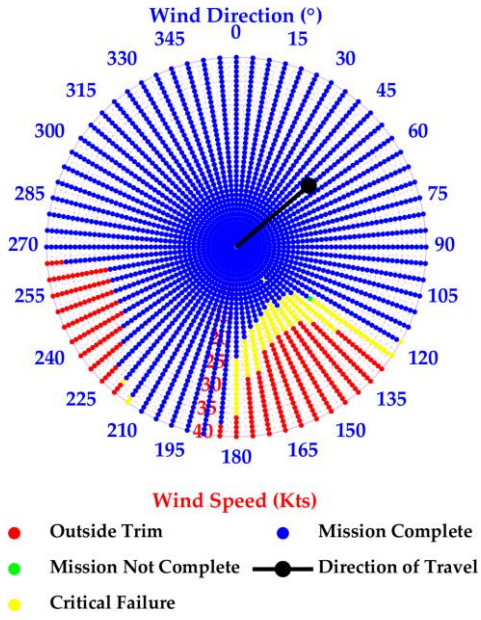

Figure 17: Simulation outcome tracking for the non- linear model simulations

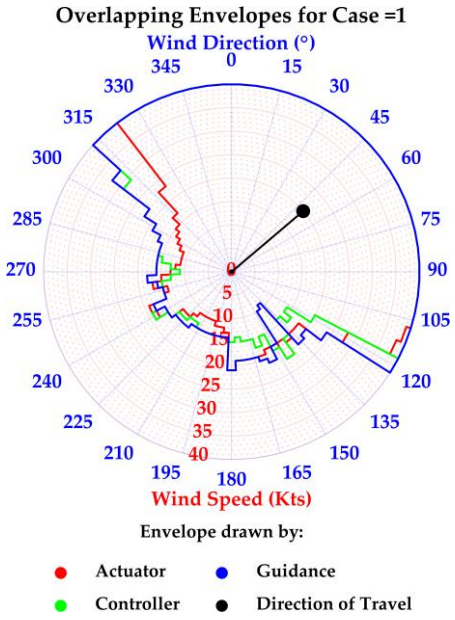

Figure 18: Subsystem envelopes for the linear model simulations

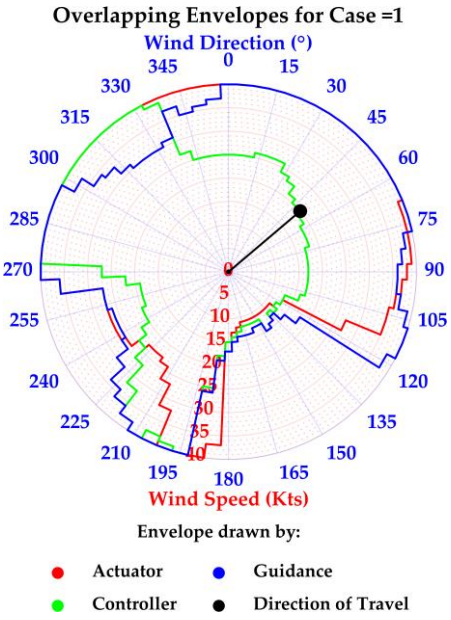

Figure 19: Subsystem envelopes for the non-linear model simulations

3.4. Comparison Near boundary

In Figure 20 through Figure 22 a closed loop comparison is made between the models for a wind direction of 135º north and a wind speed of 10 knots. This is near the edge of the boundary shown in Figure 19. It can be seen that the agreement between the models is favourable for the ground velocities and the attitude, although not as good as the for the 1 knots wind speed case shown in Figure 13 through Figure 15. As with the previous case there are larger differences in the lateral axis.

However, when the controls are considered, there is clearly a large difference between the two models, where the linear model has a greater variance in its input and the two models differ in their magnitude. This is in contrast to the controls for the 1knot wind speed case, where there was good agreement.

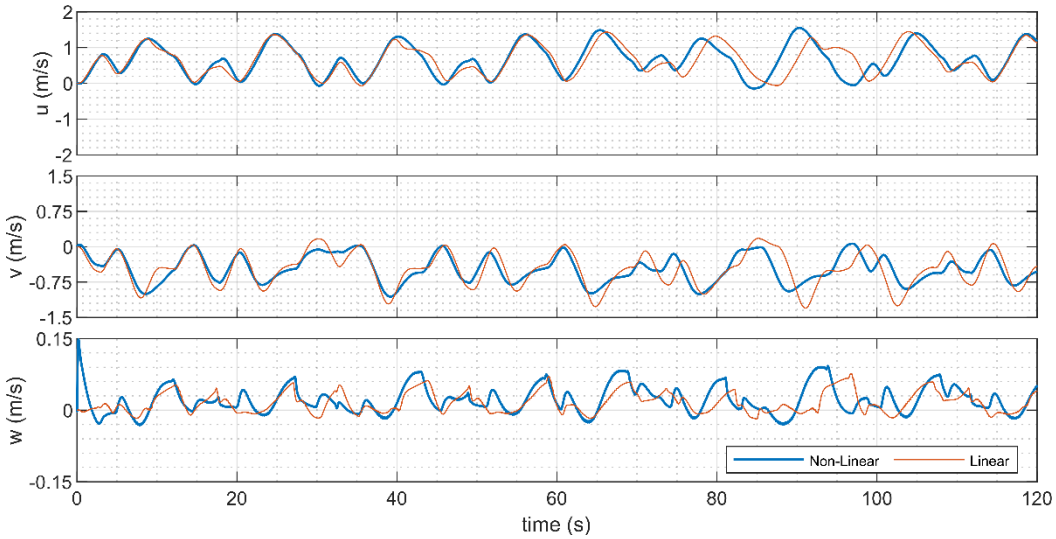

Figure 20: Closed loop response of ground velocities for linear and non-linear models $\psi_w = 135$ and $V_w = 10$

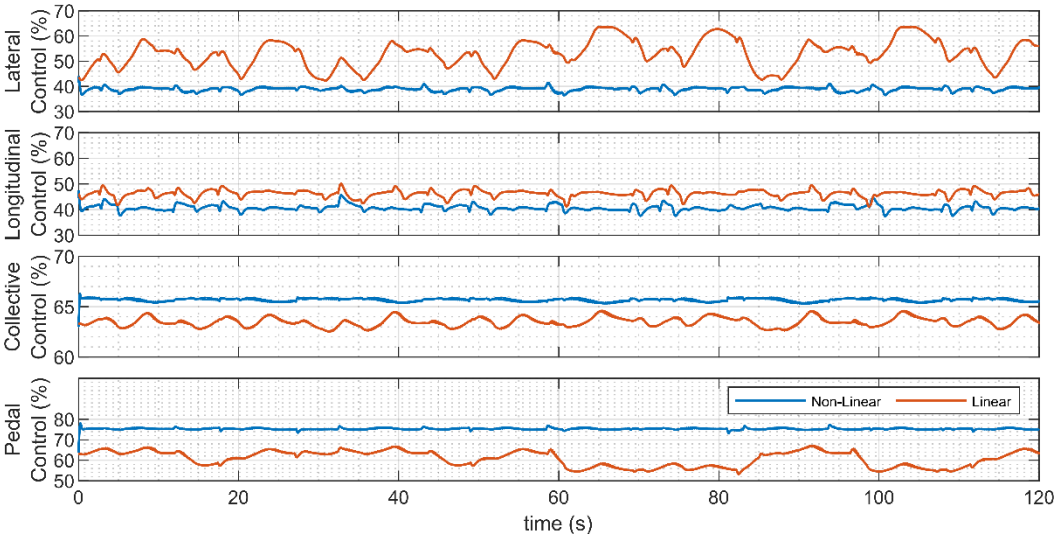

Figure 21: Closed loop response of controls for linear and non-linear models $\psi_w = 135$ and $V_w = 10$

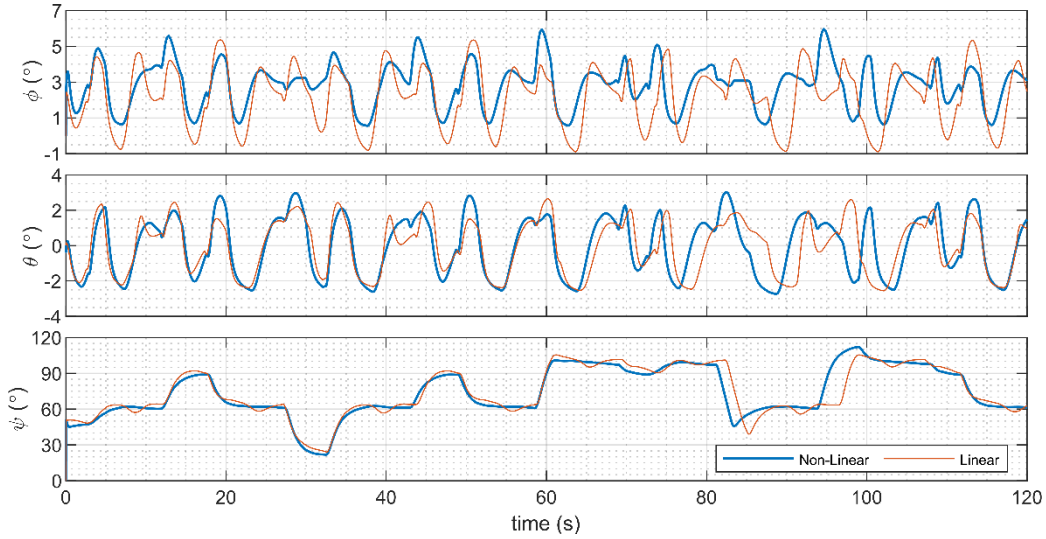

Figure 22 Closed loop response of attitude for linear and non-linear models $\psi_w = 135$ and $V_w = 10$

3.5. Final envelopes

In Figure 23 the operating envelopes for the linear and non-linear models are shown. These are the envelopes where the subsystem that has the worst performance is used as the operating limit.

It can be seen that the linear models provide a wider envelope in the north and east regions, while the non-linear provides a wider envelope in the east and south. They do, however, agree on the operating limit in the south east and south west regions. The cause of the limit, denoted by the different colours, in these regions is different.

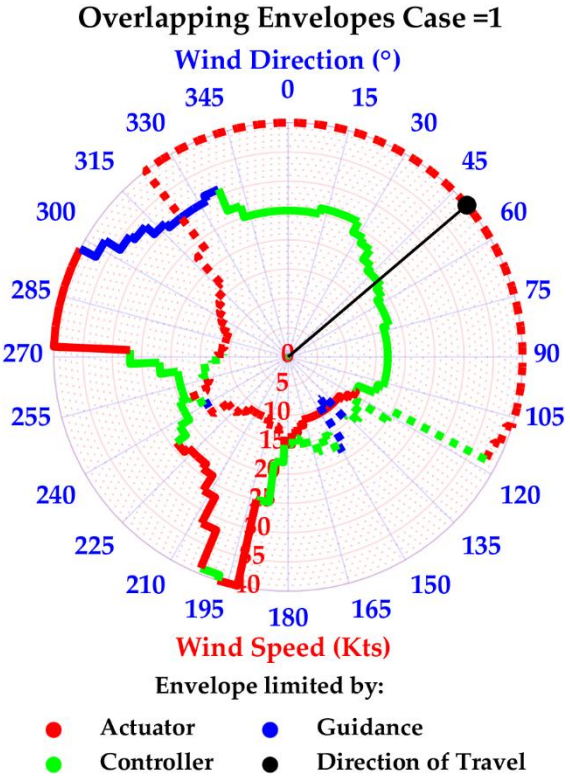

Figure 23 Envelopes when using the linear (dotted) and non-linear (solid) models.

4. DISCUSSION

From the open loop response shown in section 3.1 and the closed loop response shown in section 3.2 the linear and non-linear models appear to compare favourably and the stitched linear model would appear to make a reasonable substitute for the non-linear models. However, when viewing the envelopes, this is not the case.

The envelopes seem to agree when the helicopter is in a head wind, for the actuator and guidance subsystem. While for tail and cross winds there is little agreement over 10 knot wind speeds. This is borne out even when the envelope is limited by subsystem as in section 3.5. This implies that for the benign cases, in this case <10 knots, the linear models could be used as a substitute, while for the harsher wind conditions, the non-linear models are required to determine the operating envelope.

The continued favourable agreement when viewing the velocities and attitudes as the wind speed is increased from 1 knots to 10 knots, comparing Figure 13 to Figure 20 and Figure 15 to Figure 22, is likely due to the controller. Each model is tasked with the same mission, so the headings and velocities from the guidance should be very similar if the mission is successful. The controller is then using more control input to force the system to track those states. The extra difference in the tracked variables are then picked up by the controller cost function and result is a lower calculated performance. Hence, the control inputs are much more different for the 10 knots over the 1 knots case. The controller is in essence compensating for the differences in dynamics. The use of the cost functions allows this to be borne out on the macro scale of a range of conditions, over requiring the inspection of the responses of multiple missions

The higher variance in the controls at higher wind speeds is likely due to non-linearity in the model increasing roll and pitch rates over time, whereas linear models can only produce linear responses by definition. As a result, the controller must ask for more control input to achieve the same accelerations for the linear models.

The differences in the south and west regions of Figure 18 and Figure 19 are likely due to the models being stitched using only forward flight speed, wind speed and wind direction. When flying in the presence of wind, the guidance system attempts to tack into the wind as well as roll into it. This results in the helicopter having a significant lateral velocity component when flying in a cross wind. To improve the linear models when in cross winds the lateral velocity should be included within the stitching process.

5. CONCLUSIONS

This paper aimed to use linear and non-linear aircraft models to create operating envelopes of an oil rig inspection mission. This is to determine whether or not the more computationally expensive non-linear models are required to create the operating envelope. Thus, the following conclusions are be drawn:

1. For benign wind conditions, <10 knots wind speed, the use of linear models appears to be sufficient to provide an estimate of the UAS's operating envelope. However, greater than this and the non-linear models are required.

2. The differences between the linear and non-linear models for the benign wind conditions appear to exist on the lateral axis, where agreement for ϕ and v are poor. This is likely due to the models being stitching using wind speed, wind direction and forward ground speed only, where the impact of the lateral ground velocity is not accounted for.
3. The non-linear models appear to require more control input to maintain stability and tracking control of the UAS. This then causes the control metric to drop and reduce the overall operating envelope.

There are several possible areas of future work that follow on from the work presented here:

1. Include the lateral ground speed of the aircraft in the stitching process in order to improve agreement during benign conditions and to potentially expand the wind speeds at which the linear models can be applied.
2. Investigate whether the linear models can be used to obtain a 'first estimate' of the operating envelope and then apply the non-linear model. Thus, a two-step process is used to determine the operating envelope, but at a reduced computational cost.
3. Recompute operating envelopes with the turbulent air wake of the oil rig itself integrated into the nonlinear simulation model

6. REFERENCES

[1] UK-RAS Network, 'White Paper: Robotics & Autonomous systems: Challenges and Opportunities for the UK'. 2018.

[2] G. D. Carico, R. Fang, R. S. Finch, W. P. Geyer Jr, H. W. Krijins, and K. Long, 'Helicopter/Ship Qualification Testing: Part 1 Ductch/British Clearance Process', *NATO RTO*, vol. 22, pp. 13–23, 2003.

[3] J. Forrest, S. J. Hodge, I. Owen, and G. D. Padfield, 'Towards fully simulated ship-helicopter operating limits: The importance of ship airwake fidelity', *American Helicopter Society 64th Annual Forum*, Apr. 2008.

[4] J. Forrest, I. Owen, G. D. Padfield, and S. J. Hodge, 'Ship Helicopter Operating Limits Prediction Using Piloted Flight Simulation and Time-Accurate Airwakes', *Journal of Aircraft*, vol. 49, no. 4, pp. 1020–1031, Jun. 2012.

[5] I. Owen, M. D. White, G. D. Padfield, and S. J. Hodge, 'A virtual engineering approach to the ship-helicopter dynamics interface - A decade of modelling and simulation research at the University of Liverpool', *The Aeronautical Journal*, vol. 121, no. 1246, pp. 1833–1857, 2017.

[6] S. J. Hodge, J. Forrest, G. D. Padfield, and I. Owen, 'Simulating the Environment at the Helicopter-Ship Dynamic Interface: Research, Development and Application', *Aeronautical Journal*, vol. 116, no. 1185, pp. 1155–1184, Nov. 2012.

[7] M. Kelly, N. A. Watson, S. J. Hodge, M. D. White, and I. Owen, 'The Role of Modelling and Simulation in the Preparations for Flight Trials Aboard the Queen Elizabeth Class Aircraft Carriers', *14th International Naval Engineering Conference, The Institute of Marine Engineering, Science and Technology (IMarEST)*, Oct. 2014, [Online]. Available: https://doi.org/10.24868/issn.2515-818X.2018.037

[8] V. Page, M. Webster, M. Fisher, and M. Jump, 'Towards a Methodology to Test UAVs in Hazardous Environments', *ICAS 2019, The Fifteenth International Conference on Autonomic and Autonomous Systems, Athens, Greece,* pp. 38–45, Jun. 2019.

[9] V. Page, C. Dadswell, and M. Jump, 'A Manned Aviation-Inspired Simulation Method to Determine the Operating Envelopes for Autonomous UAS in Offshore Inspection Missions (in preparation)', *MDPI Robotics Special Issue - Advances in Robots for Hazardous Environments in the UK*, May 2021.

[10] R. Du Val and C. He, 'Validation of the FLIGHTLAB Virutal Engineering Toolset', *The Aeronatuical Journal*, vol. 122, no. 1250, pp. 519–555, 2018.

[11] Advanced Rotorcraft Technology, Inc., 'The Scope Language Reference Manual'. Oct. 2011.

[12] H. Purnawan and M. Mardlijah, 'Design of linear quadratic regulator (LQR) control system for flight stability of LSU-05', *Journal of Physics: Conference Series 890*, 2017.

[13] MathWorks, 'Parallel Computing Toolbox: User's Guide, R2021a'.